RSC Advances

PAPER

View Article Online
View Journal | View Issue

Cite this: *RSC Adv.*, 2021, **11**, 22618

One-pot, ligand-free, room-temperature synthesis of Au/Pd/ZnO nanoclusters with ultra-low noble metal loading and synergistically improved photocatalytic performances†

Yunwei Wei, *[a] Malik Zeeshan Shahid,[b] Shujuan Lyu,[a] Weiying Sun[a] and Shuqiang Lyu[c]

Received 16th April 2021
Accepted 15th June 2021

DOI: 10.1039/d1ra02958d

rsc.li/rsc-advances

Au/Pd/ZnO nanoclusters with ultra-low noble metal loadings were prepared by a one-step and ligand-free method at room temperature. HRTEM, ICP-MS, XPS, and elemental mapping analysis confirmed that the obtained Au/Pd/ZnO nanoclusters were composed of ZnO nanoclusters decorated with well-dispersed AuPd nanoparticles. Au/Pd/ZnO nanoclusters exhibited higher photocatalytic activity compared with those of pristine ZnO, Au/ZnO and Pd/ZnO. Moreover, the high catalytic activity of Au/Pd/ZnO nanoclusters could be maintained even after 5 cycles of photocatalytic reaction. A mechanism for the enhanced photocatalytic performance was also suggested, which was in light of the synergistic effects of the SPR effect from Au and the improved photogenerated charge carrier separation from Pd.

1. Introduction

Over the past few decades, environmental pollution has increased seriously with the development of industry and the economy of human activities, which has motivated people to explore efficient technologies for remedying environmental pollution.[1–4] Semiconductor photocatalysis is one of the advanced physicochemical processes applicable in the photodegradation of environmental pollutants and toxic compounds, because it is an energy-saving, environmentally friendly and efficient technology in comparison with other techniques.[5–7] Among the photocatalysts, zinc oxide (ZnO) has attracted considerable attention due to its low cost, nontoxicity, abundance, wide band gap, and unique optical and electronic properties.[8–10] However, the pristine ZnO usually exhibits low photo energy conversion efficiency probably because of its relatively low charge separation efficiency and fast recombination of photogenerated electron–hole pairs.[11,12]

A number of efforts have been devoted to improving the photocatalytic performance ZnO, such as constructing nanostructures,[13–16] coupling of ZnO with another semiconductor,[17–19] doping with metal or non-metal elements,[20,21] and decorating with noble metals.[22–42] In the last case, the decoration of noble metals (Au, Pt, Ag, and Pd) on ZnO can act as sinks for the photogenerated electron in order to prolong the life time of electron–hole pairs.[22–26] Furthermore, noble metals (especially Au) can extend the light absorption and facilitate the creation of electron/hole pairs due to their surface plasmon resonance (SPR) effect.[25–27] Meanwhile, Pd nanoparticles (NPs) has a higher electron trapping capability than Au and Ag NPs and consequently improves photocatalytic activity by inhibiting the recombination of photoinduced electron–hole pairs.[28–30] Hence, the combination of ZnO with noble metals to form noble metal/semiconductor hybrid nanostructures has been proposed as an efficient way to increase photocatalytic efficiency.[31–33] Bimetallic (such as AuPd,[24,28–30,34,35,42] AuPt,[36–39] AgPd[40,41]) NPs couple with semiconductors have better performance in comparison with monometallic NPs due to the synergistic effects. In particular, AuPd NPs have been proved to promote the photochemical activity significantly. Li had synthesized the well-defined Au@ZnO–Pd core–shell nanostructures by coating ZnO on cetyltrimethylammonium bromide (CTAB) stabilized Au nanospheres in aqueous solution and subsequently loading ~1.8 wt% Pd NPs by a photo-deposition process. The obtained Au@ZnO–Pd photocatalyst exhibited the improved photocatalytic activities than those of Au@ZnO and ZnO–Pd.[28] Pankaj Singh Chauhan used 1D nanostructures of ZnO as support, and then coated more than 10 wt% Au/Pd NPs to strengthen the photocatalytic performance by using a sputtering technique.[24] In another case, Au/Pd NPs (1 wt% of total metal) decorate TiO_2 were successfully synthesized by using PVA as ligand and provide extraordinarily high efficiencies for the photocatalytic

[a]Shandong Key Laboratory of Biophysics, Institute of Biophysics, Dezhou University, Dezhou 253023, Shandong, P. R. China. E-mail: sdweiyunwei@163.com
[b]School of Chemistry and Chemical Engineering, University of Jinan, Jinan 250022, Shandong, P. R. China
[c]School of Mechanical Engineering, Chungbuk National University, Cheongju, Chungbuk 28644, Repulic of Korea

† Electronic supplementary information (ESI) available. See DOI: 10.1039/d1ra02958d

H_2 production compared with their monometallic counterparts.[33] In consideration of the scarcity and high price of noble metals, minimizing the metal loading on semiconductor photocatalysts in order to improve their photocatalytic performance and stability is of vital importance for environment remediation. However, as far as we know, to improve their photocatalytic performance of the noble metal/semiconductor hybrid photocatalysts, all the photocatalysts possess relatively high noble-metal contents range from about 1 wt% to over 20 wt%,[22–42] meanwhile the surfactants and complex steps are indispensable in the synthesis process. Hence, finding a best way to balance the noble metal loading and photocatalytic performances is urgently to be solved.

In the work, we first reported the ultra-low noble metal loaded (0.2 wt% of total metal content) Au/Pd/ZnO nanoclusters which were simply synthesized by a one-pot and ligand-free approach at room temperature. The as-prepared Au/Pd/ZnO nanoclusters exhibited extremely high photocatalytic activity and stability compared with those of pristine ZnO or the corresponding monometallic decorated ZnO counterparts. A mechanism for the enhanced photocatalytic performance was also suggested, which was in light of the synergistic effects of the SPR effect from Au and the improved photogenerated charge carriers separation from Pd. The ultra-low noble metal loading and facile synthesis method make Au/Pd/ZnO nanoclusters possessing great potential for practical application in photocatalytic degradation of pollutants.

2. Experimental section

2.1. Chemicals

Ethanol (99.7%) and ethylene glycol (EG, 99.8%) were purchased from Xilong Chemical Industry Incorporated Co. Ltd. Zinc nitrate hexahydrate ($Zn(NO_3)_2 \cdot 6H_2O$, 99.0%), sodium hydroxide (NaOH, 96.0%), benzoquinone (BQ, 97%), isopropyl alcohol (IPA, 98%), disodium ethylenediaminetetraacetate (EDTA-2Na, 98%), rhodamine B (RhB, 98%), and methyl orange (MO, 98%) were purchased from Sinopharm Chemical Reagent Co. Ltd. Chloroauric acid ($HAuCl_4$, 99.9%), sodium tetrachloropalladate (Na_2PdCl_4, 99.9%) were purchased from Sigma-Aldrich. Deionized water was prepared with a Milli-Q water purification system (LCT-I-10/20T). All reagents were analytical grade and used as received without further purification.

2.2. Synthesis of ZnO, Au/ZnO, Pd/ZnO and Au/Pd/ZnO nanoclusters

In a typical procedure, 20 mL of 0.5 M $Zn(NO_3)_2 \cdot 6H_2O$ aqueous solution was added into 160 mL EG with vigorously stirring. Subsequently, 0.62 mL of 10 mM $HAuCl_4$ and 0.38 mL of 10 mM Na_2PdCl_4 aqueous solution were introduced into the above solution. After stirring for 3 min, 20 mL of 2.5 M NaOH aqueous solution was swiftly injected, and the color of the solution gradually changed from colorless to dark reddish purple within the initial 10 min, indicating the formation of Au/Pd/ZnO. The final concentrations of $Zn(NO_3)_2$, $HAuCl_4$, Na_2PdCl_4, and NaOH were 50, 0.031, 0.019, and 250 mM, respectively. Finally, the above mixture solution was stirred for 60 min at room temperature and the products were collected by centrifugation and washed with absolute ethanol for 3 times. The final products displayed in Fig. 1 were obtained by drying at 40 °C overnight. For comparison, pristine ZnO nanoclusters without introducing $HAuCl_4$ and Na_2PdCl_4, Au/ZnO nanoclusters with only utilization of 0.82 mL of 10 mM $HAuCl_4$ aqueous solution, and Pd/ZnO nanoclusters with addition of 1.52 mL of 10 mM Na_2PdCl_4 aqueous solution, in the reaction precursor were also prepared using the similar procedure described above. Note that the noble metal loadings in all the catalysts were expressed as the noble metal/ZnO wt% ratio. The noble metal loadings of all catalysts were 0.2 wt% and the mass ratio between the Au and Pd was 3 : 1. Schematic illustration for the synthesis of Au/Pd/ZnO nanoclusters was shown in Fig. S1.†

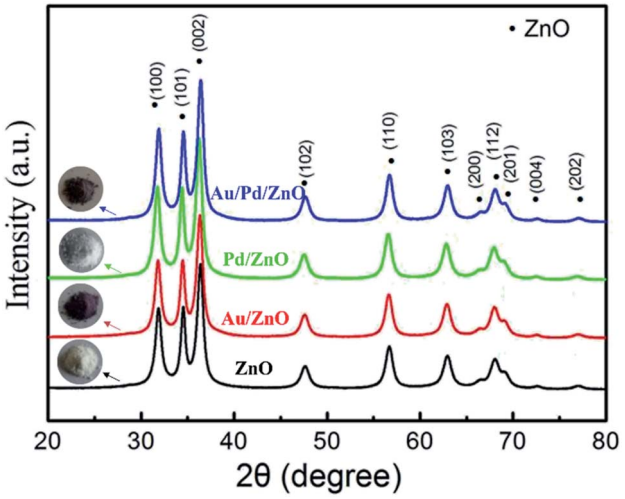

Fig. 1 XRD patterns of ZnO, Au/ZnO, Pd/ZnO, and Au/Pd/ZnO nanoclusters. The insets are photographs under the ambient light illumination of the as-prepared samples.

2.3. Characterization

X-ray diffraction (XRD) patterns were recorded on a Bruker D8 ADVANCE X-ray diffractometer with Cu Kα radiation ($\lambda = 1.5418$ Å). The morphologies of the products were characterized by transmission electron microscopy (TEM, JEOL JEM-2100F) employing an accelerating voltage of 200 kV. The samples for TEM observations were prepared by putting the products on a thin carbon film coated copper grids. High-resolution transmission electron microscopy (HRTEM) imaging and energy-dispersive X-ray (EDX) elemental mapping were carried out on JEOL JEM-2010F. X-ray photoelectron spectroscopy (XPS) data were obtained on an Escalab 250Xi instrument from Thermo Fisher Scientific using monochromatic Al Kα radiation. To compensate for surface charging effects, the binding energies were calibrated using the C 1s hydrocarbon peak at 284.80 eV. UV-Vis-NIR diffuse reflectance spectra (DRS) were performed on a Shimadzu UV-3101PC. Photoluminescence (PL) measurements were carried out on an Edinburgh FLS980 fluorescence spectrophotometer. The Pd and Au contents in Au/Pd/ZnO

nanoclusters were measured by inductively coupled plasma mass spectra (ICP-MS) on a Thermo Scientific X Series-II mass spectrometer.

2.4. Photocatalytic activity measurements

The photocatalytic activities of as-prepared samples were tested by degrading organic dyes (RhB and MO) in aqueous solution at ambient condition. In the photocatalytic experiments, 8 mg of as-synthesized samples were added in a beaker containing 29.7 mL deionized water, forming a suspension under a magnetic stirring. Subsequently, 0.3 mL of 1 mM organic dyes aqueous solution was introduced into the above suspension. The obtained mixture was stirred in the dark to reach adsorption–desorption equilibrium between the catalyst and organic dyes. Then, the mixture was irradiated by a 300 W xenon lamp without using filters and the irradiation range from 190 to 1100 nm. The photocatalytic degradation process was monitored using a UV-Vis spectrophotometer (Shimadzu UV-3101PC) to record the characteristic absorption of RhB (550 nm) and MO (470 nm).

Controlled photocatalytic activity experiments using different radical scavengers (EDTA-2Na, IPA, and BQ as scavengers for photogenerated hole, $^{\bullet}OH$ radical, and $^{\bullet}O^{2-}$ radical, respectively[28,43]) were performed similar to the above photocatalytic experiments except that the radical scavengers (10 mM) were added to the reaction system.

The recycled photocatalytic activity test was carried out to investigate the photocatalytic durability of Au/Pd/ZnO nanoclusters following a similar procedure described above. Briefly, a suspension containing Au/Pd/ZnO nanoclusters and RhB were firstly stirred in the darkness for 1 h and then illuminated for 10 min under a 300 W xenon lamp. Then, 2 mL suspension was sampled to measure the degradation effect of RhB. Meanwhile, a certain amount of RhB aqueous solution was introduced into the remaining suspension for the recycled degradation experiment. Note that the initial RhB concentration in the cyclic degradation experiments was always kept at 0.01 mM.

3. Results and discussion

3.1. Structure and morphology

The XRD patterns and photographs under the ambient light illumination of the as-prepared ZnO, Au/ZnO, Pd/ZnO, and Au/Pd/ZnO nanoclusters were shown in Fig. 1. The color of the as-prepared ZnO sample appeared to white under the ambient light illumination and the diffraction peaks of the sample shown in Fig. 1 were in good agreement with the hexagonal wurtzite crystal structure of ZnO (JCPDS no. 36-1451). Meanwhile, the color of the as-prepared Au/ZnO, Pd/ZnO, and Au/Pd/ZnO samples had a marked color evolution changing from modena, lightgray to lilac (insets in Fig. 1). Interestingly, although a remarkable color evolution of the as-synthesized samples, the diffraction peaks are all attributed to the hexagonal wurtzite crystal structure of ZnO and no peaks associated with Au or Pd NPs were detected in the XRD patterns (Fig. 1), possibly due to the low loading contents, small particle size and high dispersity of noble metal NPs.[44,45] In order to quantify the deposited Au and/or Pd contents in ZnO nanoclusters, inductively coupled plasma mass spectrometer analysis was performed. The ICP-MS data demonstrated that Au and/or Pd contents in ZnO nanoclusters were in well-matched with those of initial value in starting materials (Table S1†).

The morphological features of the obtained ZnO, Au/ZnO, Pd/ZnO, and Au/Pd/ZnO nanoclusters were further characterized by TEM and showed in Fig. 2. It was found that although the compositions of the samples were different, all the samples were nanoclusters with the size between 50 to 100 nm. Specifically, small Au or/and Pd NPs about 2–5 nm are homogeneously distributed in the whole nanoclusters, suggesting the Au or/and Pd NPs were well-decorated on ZnO. HRTEM images in Fig. 2e demonstrated that the adjacent lattice fringes of 0.248 nm which were well indexed to the lattice spacing of (101) plane of ZnO, meanwhile the interplanar distances measured from a single AuPd nanoparticle was 0.230 nm, which corresponded to the mean value of (111) planes of face-centred cubic (fcc) Au and Pd.[46] To further investigate the elemental distribution of Au and Pd in the Au/Pd/ZnO nanoclusters, elemental mappings were collected. As shown in Fig. S2,† Au and Pd were evenly distributed throughout the entire sample, indicating the AuPd NPs were well-deposited on ZnO nanoclusters.

To understand the surface composition and elemental chemical states of the Au/Pd/ZnO sample, XPS analysis of the as-obtained products were collected. As shown in Fig. 3a, the survey spectrum exhibited obvious signals of Zn and O elements, but the signals of Au and Pd were negligible due to their low loading. In the high-resolution spectrum of Zn 2p (Fig. 3b), the peaks with binding energies of 1021.3 eV and 1044.4 eV were attributed to Zn $2p_{3/2}$ and Zn $2p_{1/2}$ for Zn^{2+} of ZnO.[47] Meanwhile, the O 1s spectrum exhibited three peaks centered at 529.1, 530.7 and 531.37 eV (Fig. 3c), which were attributed to the lattice oxygen (529.1 eV) and the oxygen deficient region (530.7 and 531.37 eV) in ZnO, respectively.[48] As presented in Fig. 3d, the peaks located at 88.13 eV can be indexed to Au $4f_{5/2}$, moreover, it should be noted that other peak

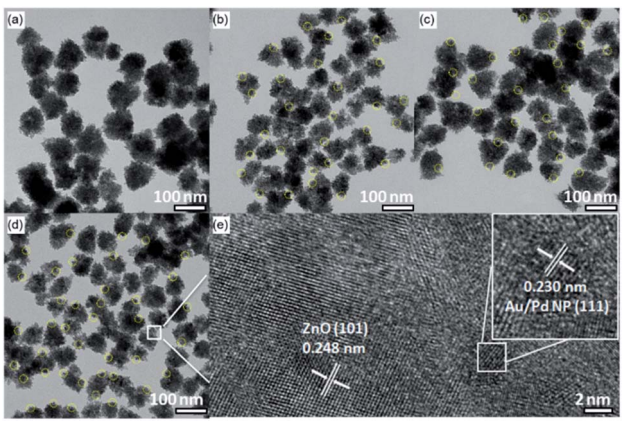

Fig. 2 TEM images of (a) ZnO, (b) Au/ZnO, (c) Pd/ZnO, and (d) Au/Pd/ZnO. (e) HRTEM image of as-prepared Au/Pd/ZnO. Yellow dashed circles in (b), (c) and (d) highlight Au, Pd and AuPd NPs, respectively.

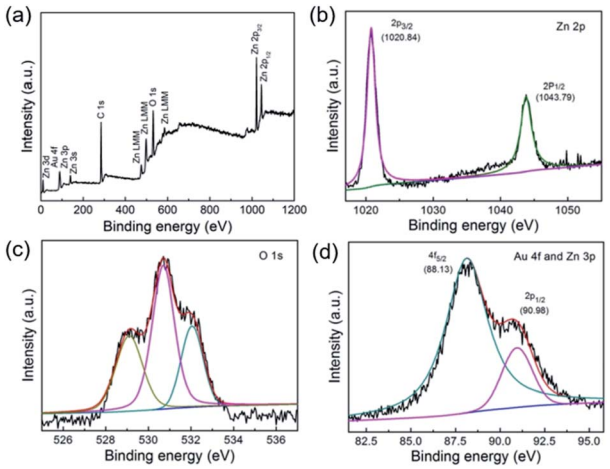

Fig. 3 XPS spectra of Au/Pd/ZnO nanoclusters: (a) wide, (b) Zn 2p, (c) O 1s, (d) Au 4f and Zn 3p.

centered at 90.95 eV are ascribed to Zn $3p_{1/2}$, similar to the previously reported literatures.[49,50] While, the Pd element was hardly detected by XPS characterization because the signal of Pd was very weak due to its low loading content (less than 0.05 wt%). The above results confirmed that the obtained Au/Pd/ZnO nanoclusters were composed of ZnO nanoclusters decorated with well-dispersed AuPd nanoparticles with ultra-low noble metal loading and small particle size.

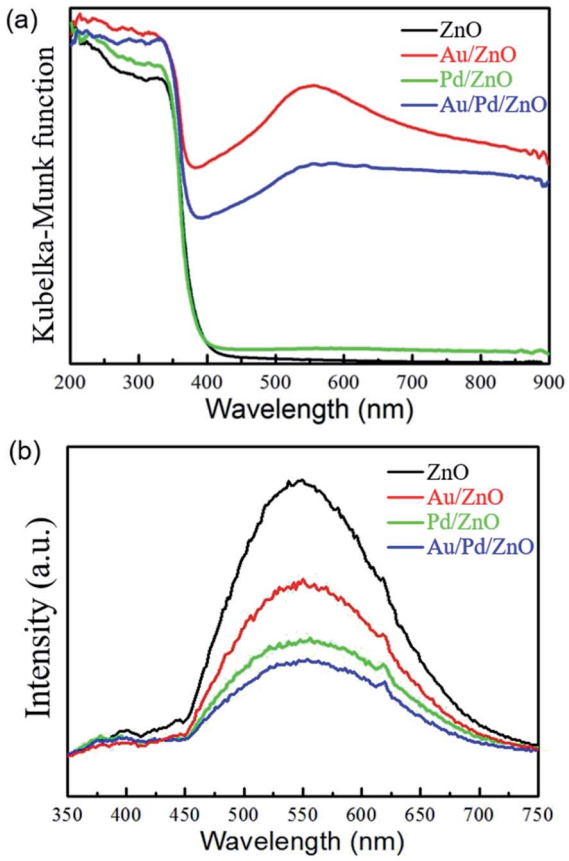

Fig. 4 (a) UV-Vis diffuse reflectance spectra, and (b) PL emission spectra of pristine ZnO (black), Au/ZnO (red), Pd/ZnO (green), and Au/Pd/ZnO (blue).

UV/Vis spectra of as-prepared the samples were further investigated. As shown in Fig. 4a, the as-prepared ZnO, Au/ZnO, Pd/ZnO and Au/Pd/ZnO samples both exhibited a strong absorption in the ultraviolet region (λ < 360 nm), showing that the intrinsic bandgap of ZnO was not changed after decorating it with Au and/or Pd NPs. Interestingly, both Au/ZnO and Au/Pd/ZnO displayed a prominent absorption band in the range of 400–900 nm which could be ascribed to the SPR effect of Au NPs in the as-prepared sample.[28,33] Hence, the decoration of Au and AuPd NPs could significantly improve the light absorption intensity of the samples in the visible region, which had the potential of enhancing photochemical activity.

Considering the comparable UV light absorption capability of Au/ZnO nanoclusters and Au/Pd/ZnO nanoclusters, the charge separation and transfer efficiency of the different photocatalysts could be revealed by their photoluminescence (PL) emission spectra. Generally speaking, a lower recombination of photogenerated electron–hole pairs were caused by a lower PL emission intensity.[30] As shown in Fig. 4b, the pristine ZnO nanoclusters presented the highest PL emission intensity, suggesting the largest recombining probability of the photogenerated carriers in this sample. The PL emission intensity of the ZnO nanoclusters was quenched by decorated with Au NPs in a large degree, and further quenched by loading Pd NPs. It was interesting that the PL emission intensity of Au/Pd/ZnO nanoclusters was greatly decreased compared with its monometallic counterparts, indicating the recombination of the photogenerated electron–hole pairs was greatly suppressed in the bimetallic systems.[24,28,34] Combined the results of UV-Vis diffuse reflectance spectra and PL emission spectra, the enhanced light absorption and suppression of the photogenerated electron–hole pairs recombination were expected to give an improved solar energy utilization efficiency in the photocatalysis process, possibly providing a superior photocatalytic performance.

3.2. Photocatalytic performance

The photocatalytic activities of Au/Pd/ZnO nanoclusters were evaluated by decomposing RhB in aqueous solutions using a 300 W xenon lamp as the simulated solar light source. The photocatalytic activities of ZnO, Au/ZnO, Pd/ZnO nanoclusters were also tested for comparison. Before the photocatalytic experiments, the solution was stirred in the dark for 1 h to reach adsorption–desorption equilibrium between the samples and RhB (Fig. S3a†), and the evolutions in the absorption spectra of RhB solutions along with the irradiation time in the presence of different samples were shown in Fig. S3.† The sample without catalyst shown a strong absorption peak centered at about 550 nm, and the photolysis of RhB could be ignored (Fig. S3b†). For ZnO nanoclusters, the photocatalytic conversion of RhB was only reduced to 74.4% after 10 min irradiation (Fig. S3c†). As shown in Fig. 5b, the distinctly enhanced photocatalytic efficiencies were observed with the addition of Pd/ZnO, Au/ZnO,

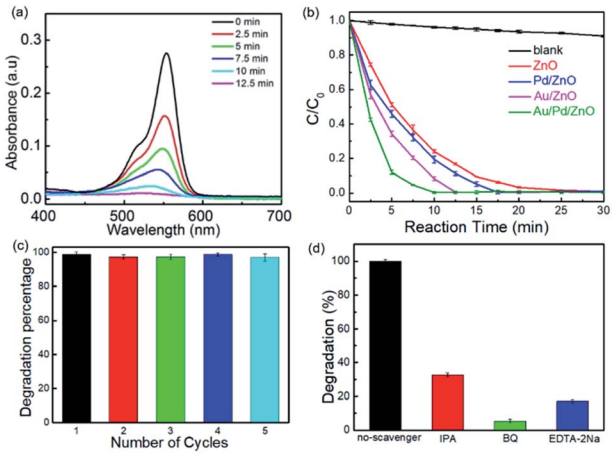

Fig. 5 (a) UV-Vis spectral evolution of RhB aqueous solution in the presence of Au/Pd/ZnO, (b) the photocatalytic performances (C/C_0) of blank and as prepared ZnO, Au/ZnO, Pd/ZnO, and Au/Pd/ZnO samples for degradation of RhB under simulated solar light irradiation, (c) the multicycle degradation results of RhB catalyzed by Au/Pd/ZnO, (d) photocatalytic degradation of RhB in the presence of different scavengers by Au/Pd/ZnO under simulated solar irradiation. Blank in (b) is UV-Vis spectra evolution of RhB aqueous solution under photo-illumination in the absence of catalyst.

and Au/Pd/ZnO, which is evidenced by the increased degradation rates of RhB for the samples. Especially, AuPd NPs modified ZnO photocatalyst exhibited superior photocatalytic activity for degrading RhB in comparison with others, where RhB was almost completely degraded by Au/Pd/ZnO within 10 min (Fig. 5a). In contrast, the photocatalytic conversions of RhB were reduced to 80.3% and 91.2% for Pd/ZnO and Au/ZnO, respectively. More details about the time-dependent photocatalytic degradation profiles were available in Fig. S3c–f.† The improved degradation efficiency of Au/ZnO and Pd/ZnO could be ascribed to the surface plasmon resonance effect of Au NPs and the photogenerated charge carriers separation which due to electron-sink function of Pd NPs. The further improved photocatalytic activity of Au/Pd/ZnO was possibly due to the bimetallic decoration which possessed not only the SPR effect but also had the combined effect to scavenge electron from the conduction band before their recombination with holes.[24,28] In addition, the reusability of Au/Pd/ZnO nanoclusters were also investigated by performing 5 cycles of photodegradation experiment were presented in Fig. 5c. The result showed that the degradation rate maintains at above 95% even after 5 cycles of degradation. Moreover, TEM observations of the as-synthesized Au/Pd/ZnO catalysts recovered after cycling photocatalytic reaction for organic dye RhB under the irradiation with xenon lamp indicate that the size and structure of the as-prepared catalysts remained essentially unchanged after the photocatalytic reactions (Fig. S4†), which demonstrate the as-prepared catalysts have a good durability and always keep a high catalytic activity. Interestingly, when we fixed the total amount of precious metals and used different mass ratio of Au and Pd, which found that the ratio between the bimetals had effect on the catalytic results (Fig. S5†). In the ternary hybrid nanostructures, ZnO provides the photo-generated carriers under UV-visible light, and Au nanocrystals perform the plasmonic hot electron injection. Meanwhile, the Pd NPs can efficiently trap the generated electrons to govern the directional separation of the charge carriers. In our experiment, considering the ultra-low noble metal loaded (0.2 wt% of total metal content), the SPR effect of Au NPs maybe important than the trap effect of Pd NPs. However, compared with the effect on the catalytic results between the pristine ZnO or the monometallic decorated ZnO counterparts and Au/Pd/ZnO nanoclusters, the effect on the catalytic results by different mass ratio of Au and Pd was not very remarkable. Hence, in this work, 3 : 1 was chosen as the final mass ratio between Au and Pd.

In order to examine the applicability of Au/Pd/ZnO nanocluster for degrading other water pollutant, MO was selected as a typical pollutant, and photo-catalytically degraded under the same conditions. As shown in Fig. S6,† the results of photocatalytic MO degradation over the different photocatalysts were almost coincident with those of the photocatalytic degradation of RhB, indicating that no selectivity was observed in Au/Pd/ZnO nanoclusters.

The active species in RhB degradation were examined by adding a series of scavengers, such as IPA, BQ and EDTA-2Na, which were used to trap the active hydroxyl radicals ($^{\bullet}OH$), superoxide radicals ($^{\bullet}O^{2-}$) and photogenerated holes (h^+).[34,37] As a consequence of quenching, photocatalytic oxidation reaction would be partly suppressed and the RhB conversion was lowered induced by a scavenger, illustrating the importance of the corresponding oxidizing species. The results of the photocatalytic RhB degradation with the addition of different scavengers were shown in Fig. 4d. The RhB conversion over Au/Pd/ZnO exhibits the most rapidly decrease ~94% after adding BQ, proposing the $^{\bullet}O^{2-}$ was the main active species in the photocatalytic process. After adding IPA and EDTA-2Na, the photocatalytic conversions of RhB decreased to 67% and 83%, respectively. These results indicated that $^{\bullet}OH$ and h^+ also play an important role in the oxidation of RhB. Moreover, when IPA select as a scavenger, the Au-NPs are able to abstract hydrogen from isopropanol forming the transient Au–H species under visible light irradiation which could attack the double bonds or epoxide bond leading to the hydrogenation or deoxygenation, in which the hydrogen of Au–H species is consumed and the final reductive products form without releasing hydrogen molecules.[51] Therefore, the reactive species involved in the degradation of RhB were $^{\bullet}O^{2-}$, $^{\bullet}OH$ and h^+.

3.3. Photocatalytic mechanism discussion

It had been proved that AuPd bimetallic NPs could enhance the photocatalytic activity and increase the rate of photodegradation of ZnO.[24,28,34] According to the results, a possible mechanism for the solar-light-driven Au/Pd/ZnO photocatalyst was proposed and illustrated in Fig. 6. In general, the Fermi level would be equilibrated inevitably by an interfacial charge transfer, when a metal contacted a semiconductor.[52] The work function of ZnO was about 4.65 eV, which is lower than that of Au (~5.14 eV) and Pd (~5.24 eV).[28,30] Therefore, two Schottky

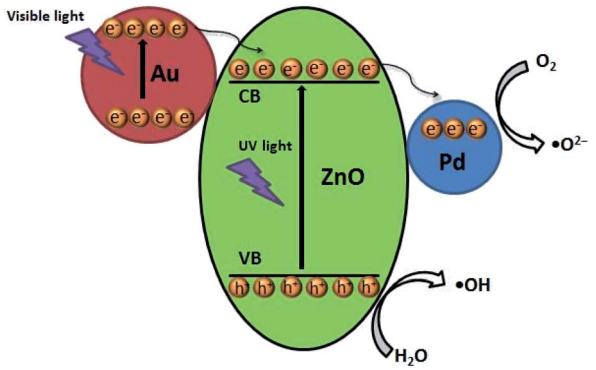

Fig. 6 Photocatalytic mechanism of Au/Pd/ZnO nanoclusters for the degradation of RhB and MB under simulated solar light irradiation.

barriers could be generated by forming Au–ZnO and Pd–ZnO interfaces.[28] Under the irradiation of visible light, the plasmonic resonance aroused from the collective oscillations of the hot electrons generated on the irradiated Au NPs and the plasmonic hot electrons from Au NPs with high energy could inject into the conduction band of ZnO.[37] This plasmonic energy transfer would remarkably increase the number of photo-generated carriers in ZnO. Simultaneously, the electrons would be trapped by Pd NPs by the Schottky barriers of Pd–ZnO. The separated electrons and holes were captured by surface-adsorbed O_2 and H_2O, respectively, to generate the reactive oxidation species of $\bullet O^{2-}$ and $\bullet OH$ radicals.[28] Finally, both active species degrade the organic pollutants.

4. Conclusions

In this work, we developed a one-pot and ligand-free approach for synthesizing the ultra-low noble metal loaded (0.2 wt% of total metal content) Au/Pd/ZnO nanoclusters at room temperature. The obtained Au/Pd/ZnO nanoclusters were composed of ZnO nanoclusters decorated with well-dispersed AuPd NPs with ultra-low noble metal loading and small particle size. The obtained Au/Pd/ZnO nanoclusters exhibited the highly photocatalytic activity and stability for degradation of RhB, and no selectivity was observed for MO. The proposed mechanism revealed that the enhanced photocatalytic performance was attributed to the synergistic effect of Au and Pd NPs, in which Au NPs provided a SPR effect and Pd NPs improved the photogenerated charge carriers separation. The obtained Au/Pd/ZnO nanoclusters could be effectively used for practical application in photocatalytic degradation of pollutants.

Conflicts of interest

There are no conflicts to declare.

Acknowledgements

This work was financially supported by National Natural Science Foundation of China (Grant No. 51671094) and Dezhou University Science Research Fund (Grant No. 2020xjrc217).

References

1 M. A. Mohd Adnan, N. M. Julkapli and S. B. Abd Hamid, *Rev. Inorg. Chem.*, 2016, **36**, 77–104.
2 K. Qi, B. Cheng, J. Yu and W. Ho, *J. Alloys Compd.*, 2017, **727**, 792–820.
3 P.-X. Li, X.-Y. Yan, X.-M. Song, J.-J. Li, B.-H. Ren, S.-Y. Gao and R. Cao, *ACS Sustainable Chem. Eng.*, 2021, **9**, 2319–2325.
4 P. Li, X. Yan, S. Gao and R. Cao, *Chem. Eng. J.*, 2021, **421**, 129870.
5 C. Chen, W. Ma and J. Zhao, *Chem. Soc. Rev.*, 2010, **39**, 4206–4219.
6 K. M. Lee, C. W. Lai, K. S. Ngai and J. C. Juan, *Water Res.*, 2016, **88**, 428–448.
7 P. Li, H. Zhao, X. Yan, X. Yang, J. Li, S. Gao and R. Cao, *Sci. China Mater.*, 2020, **63**, 2239–2250.
8 A. Sirelkhatim, S. Mahmud, A. Seeni, N. H. M. Kaus, L. C. Ann, S. K. M. Bakhori, H. Hasan and D. Mohamad, *Nano-Micro Lett.*, 2015, **7**, 219–242.
9 S. G. Kumar and K. S. R. K. Rao, *RSC Adv.*, 2015, **5**, 3306–3351.
10 R. Kumar, A. Umar, G. Kumar and H. S. Nalwa, *Ceram. Int.*, 2017, **43**, 3940–3961.
11 A. Kolodziejczak-Radzimska and T. Jesionowski, *Materials*, 2014, **7**, 2833–2881.
12 M. Ahmad and J. Zhu, *J. Mater. Chem.*, 2011, **21**, 599–614.
13 L. Wang, C. Ma, X. Ru, Z. Guo, D. Wu, S. Zhang, G. Yu, Y. Hu and J. Wang, *J. Alloys Compd.*, 2015, **647**, 57–62.
14 S. Lan, L. Liu, R. Li, Z. Leng and S. Gan, *Ind. Eng. Chem. Res.*, 2014, **53**, 3131–3139.
15 X. Jia, M. Tian, Y. Liu, X. Wu and H. Song, *Appl. Phys. A*, 2015, **119**, 1179–1185.
16 S. Dilger, M. Wessig, M. R. Wagner, J. S. Reparaz, C. M. Sotomayor Torres, L. Qijun, T. Dekorsy and S. Polarz, *Cryst. Growth Des.*, 2014, **14**, 4593–4601.
17 W. K. Jo and N. Clament Sagaya Selvam, *J. Hazard. Mater.*, 2015, **299**, 462–470.
18 S. Kuriakose, B. Satpati and S. Mohapatra, *Phys. Chem. Chem. Phys.*, 2014, **16**, 12741.
19 L. Wang, S. Liu, Z. Wang, Y. Zhou, Y. Qin and Z. L. Wang, *ACS Nano*, 2016, **10**, 2636–2643.
20 V. Kumari, A. Mittal, J. Jindal, S. Yadav and N. Kumar, *Front. Mater. Sci.*, 2019, **13**, 1–22.
21 K. Qi, X. Xing, A. Zada, M. Li, Q. Wang, S.-y. Liu, H. Lin and G. Wang, *Ceram. Int.*, 2020, **46**, 1494–1502.
22 W. He, H. K. Kim, W. G. Wamer, D. Melka, J. H. Callahan and J. J. Yin, *J. Am. Chem. Soc.*, 2014, **136**, 750–757.
23 V. V. Kondalkar, L. T. Duy, H. Seo and K. Lee, *ACS Appl. Mater. Interfaces*, 2019, **11**, 25891–25900.
24 P. S. Chauhan, A. Rai, A. Gupta and S. Bhattacharya, *Mater. Res. Express*, 2017, **4**, 055004.
25 O. Lupan, V. Postica, N. Wolff, J. Su, F. Labat, I. Ciofini, H. Cavers, R. Adelung, O. Polonskyi and F. Faupel, *ACS Appl. Mater. Interfaces*, 2019, **11**, 32115–32126.
26 Y. Chen, D. Zeng, K. Zhang, A. Lu, L. Wang and D. L. Peng, *Nanoscale*, 2014, **6**, 874–881.

27 R. Kavitha and S. G. Kumar, *Mater. Sci. Semicond. Process.*, 2019, **93**, 59–91.
28 B. Li, R. Wang, X. Shao, L. Shao and B. Zhang, *Inorg. Chem. Front.*, 2017, **4**, 2088–2096.
29 B. Bachiller-Baeza, A. Iglesias-Juez, G. Agostini and E. Castillejos-López, *Catal. Sci. Technol.*, 2020, **10**, 2503–2512.
30 R. Zhao, X. Sun, Y. Jin, J. Han, L. Wang and F. Liu, *J. Mater. Sci.*, 2019, **54**, 5445–5456.
31 J. W. Hong, D. H. Wi, S. U. Lee and S. W. Han, *J. Am. Chem. Soc.*, 2016, **138**, 15766–15773.
32 T. N. Q. Trang, T. B. Phan, N. D. Nam and V. T. H. Thu, *ACS Appl. Mater. Interfaces*, 2020, **12**, 12195–12206.
33 R. Su, R. Tiruvalam, A. J. Logsdail, Q. He, C. A. Downing, M. T. Jensen, N. Dimitratos, L. Kesavan, P. P. Wells and R. Bechstein, *ACS Nano*, 2014, **8**, 3490–3497.
34 J. Huang, J. Zhou, Z. Liu, X. Li, Y. Geng, X. Tian, Y. Du and Z. Qian, *Sensor. Actuator. B Chem.*, 2020, **310**, 127129.
35 X. Chen, Y. Shen, P. Zhou, X. Zhong, G. Li, C. Han, D. Wei and S. Li, *Sensor. Actuator. B Chem.*, 2019, **289**, 160–168.
36 J. F. S. Fernando, M. P. Shortell, K. L. Firestein, C. Zhang, K. V. Larionov, Z. I. Popov, P. B. Sorokin, L. Bourgeois, E. R. Waclawik and D. V. Golberg, *Langmuir*, 2018, **34**, 7334–7345.
37 A. Tanaka, K. Hashimoto and H. Kominami, *J. Am. Chem. Soc.*, 2014, **136**, 586–589.
38 F. Wang, Y. Jiang, D. J. Lawes, G. E. Ball, C. Zhou, Z. Liu and R. Amal, *ACS Catal.*, 2015, **5**, 3924.
39 X.-F. Zhang, Z. Wang, Y. Zhong, J. Qiu, X. Zhang, Y. Gao, X. Gu and J. Yao, *J. Phys. Chem. Solids*, 2019, **126**, 27–32.
40 H. Kahri, M. Sevim and Ö. Metin, *Nano Res.*, 2017, **10**, 1627–1640.
41 A. A. Melvin, K. Illath, T. Das, T. Raja, S. Bhattacharyya and C. S. Gopinath, *Nanoscale*, 2015, **7**, 13477.
42 Y. Lu, J. Zhang, L. Ge, C. Han, P. Qiu and S. Fang, *J Colloid Interface Sci*, 2016, **483**, 146–153.
43 H. Li, T. Hu, J. Liu, S. Song, N. Du, R. Zhang and W. Hou, *Appl. Catal. B Environ.*, 2016, **182**, 431–438.
44 G. Chen, Q. Xu, Y. Yang, C. Li, T. Huang, G. Sun, S. Zhang, D. Ma and X. Li, *ACS Appl. Mater. Interfaces*, 2015, **7**, 23538–23544.
45 B. Li, L. Shao, R. Wang, X. Dong, F. Zhao, P. Gao and Z. Li, *J. Mater. Chem. A*, 2018, **6**, 6344–6355.
46 Y. Zhang, Y. Zhang, Y. Guo, L. Wu, Y. Liu and L. Song, *RSC Adv.*, 2019, **9**, 2666–2672.
47 J. Das, S. K. Pradhan, D. R. Sahu, D. K. Mishra, S. N. Sarangi, B. B. Nayak, S. Verma and B. K. Roul, *Physica B*, 2010, **405**, 2492–2497.
48 J. Lu, H. Wang, D. Peng, T. Chen, S. Dong and Y. Chang, *Physica E*, 2016, **78**, 41–48.
49 Y. Lu, J. Zhang, L. Ge, C. Han, P. Qiu and S. Fang, *J. Colloid Interface Sci.*, 2016, **483**, 146–153.
50 T. Wang, B. Jin, Z. Jiao, G. Lu, J. Ye and Y. Bi, *J. Mater. Chem. A*, 2014, **2**, 15553–15559.
51 X. Ke, X. Zhang, J. Zhao, S. Sarina, J. Barry and H. Zhu, *Green Chem.*, 2013, **15**, 236–244.
52 Y. Sun, T. Zhang, G. Chen, F. Zhang, D. Liu, W. Cai, Y. Li, X. Yang and C. Li, *Nanoscale*, 2016, **8**, 10774.